2007

Calculation of free energies and chemical potentials for gas hydrates using Monte Carlo simulations

Peter A Monson, *University of Massachusetts - Amherst*
S. J Wierzchowski

Calculation of Free Energies and Chemical Potentials for Gas Hydrates Using Monte Carlo Simulations

S. J. Wierzchowski and P. A. Monson*

Department of Chemical Engineering, University of Massachusetts, Amherst, Massachusetts 01003

Received: December 4, 2006; In Final Form: April 6, 2007

We describe a method for calculating free energies and chemical potentials for molecular models of gas hydrate systems using Monte Carlo simulations. The method has two components: (i) thermodynamic integration to obtain the water and guest molecule chemical potentials as functions of the hydrate occupancy; (ii) calculation of the free energy of the zero-occupancy hydrate system using thermodynamic integration from an Einstein crystal reference state. The approach is applicable to any classical molecular model of a hydrate. We illustrate the methodology with an application to the structure-I methane hydrate using two molecular models. Results from the method are also used to assess approximations in the van der Waals−Platteeuw theory and some of its extensions. It is shown that the success of the van der Waals−Platteeuw theory is in part due to a cancellation of the error arising from the assumption of a fixed configuration of water molecules in the hydrate framework with that arising from the neglect of methane−methane interactions.

I. Introduction

The formation and stability of natural gas hydrates represents both an important fundamental problem in molecular thermodynamics and a problem with substantial technological importance.[1] The methane mole fraction approaching 15% in a fully occupied structure-I methane hydrate contrasts dramatically with the solubility of methane in liquid water at the same conditions that is several orders of magnitude lower. Molecular models of the interactions in water/alkane mixtures should be able to describe both phenomena. From a technological perspective, the formation of hydrates in oil and gas pipelines is an important problem in flow assurance, while the enormous hydrate deposits on ocean beds are seen as a potential fuel source much larger than other reserves of fossil fuels. Thus, gas hydrate research continues to be of wide interest.[1−4]

The hydrate complex is an assembly of cage structures created by networked water molecules around the guest molecules. The presence of guest molecules stabilizes a network of water molecules at a substantially lower water density than any of the phases of ice. Three primary structures for gas hydrates exist, structure I, structure II, and structure H.[1] Experimental studies of gas hydrates have provided information about the phase equilibrium properties,[1,5−7] the structure of the hydrate,[8,9] and the hydration number of the solid.[5,10−15] Other hydrate structures appear at high pressure as well as filled ice structures.[16,17] For the case of the structure-I methane hydrate, one unit cell of the fully occupied hydrate contains water and methane in a 46:8 ratio. However, research indicates that the methane hydrate equilibrium composition varies with the temperature and pressure with typically a small percentage of the cages empty,[5,13−15] and the impact of this upon the phase diagram has been discussed.[1,18,19] The role of the guest molecule in determining the stability of a gas hydrate is intimately linked with the physics of hydrophobic hydration in the liquid phase.[20−23] The formation of hydration shells of water around a guest molecule in the liquid phase provides a transitional structure to the water cages in gas hydrates, though a full understanding of this remains an active area of research.[15,24,25] The rigidity of the hydrogen-bonded network between the water molecules in the solid makes it possible to sustain extended arrays of guest molecules in water cages that would be suppressed by fluctuations in the liquid-phase hydrogen bond network.

In the context of statistical mechanics, the most studied methods for modeling the thermodynamics of gas hydrates are based on a formalism developed by van der Waals and Platteeuw (vdWP).[26,27] This approach approximates the gas hydrate with individual cages and noninteracting guest molecules, a formulation following from the cell theory of solids.[28,29] The success of the approach is clearly evident in that it still is the basis for industrial hydrate calculations.[1] The vdWP approach relies on four key assumptions: the contribution to the free energy from the hydrate network is independent of the hydrate occupancy, the cages are singly occupied, the guest molecule has no interaction with guest molecules in neighboring cages, and quantum effects are negligable. This leads to a factorization of the partition function into a product of cell partition functions computed from the configurations of the guest molecules in an external field created by the water molecules forming the cages. A variety of approaches have been taken to extend the vdWP theory, primarily focused on more sophisticated calculations of the cage potential energy field,[30−40] although effects such as multiple occupancy of the cages[41] and the effects of interactions between guest molecules in neighboring cages[42] have also been investigated. Tanaka et al.[41,43−46] have applied lattice dynamics to a molecular model combined with the vdWP theory to calculate hydrate free energies. This approach allows for the vibrational motion of the water molecules, but the method is limited by the range of temperature where the harmonic approximation is correct. In a similar spirit, Westacott and Rodger[47] applied a local harmonic method to calculate the direct free energy of the solid. This method does not provide for the possibility of unoccupied cages and is limited by the range of temperatures over which the approximation is correct. Monte Carlo and molecular dynamics simulations of hydrates offer the possibility of an exact calculation of the properties for a given

10.1021/jp068325a CCC: $37.00
Published on Web 05/26/2007

molecular model without the assumptions in the vdWP or lattice dynamics approaches. A variety of such calculations have been published,[37,48−64] addressing a range of issues in hydrate behavior, including assessments of the approximations built into the vdWP theory[57,59,60,64] and calculations of the vibrational spectra of the hydrate solid.[48,50,52−55,57]

Monte Carlo and molecular dynamics techniques may also be used to calculate the phase diagrams for hydrate-forming systems, but this is a significant computational undertaking that until recently has not been undertaken. In this paper, we present a methodology for calculating free energies and chemical potentials from Monte Carlo simulations of hydrates. The results from this methodology can be used to compute phase diagrams for hydrate-forming systems. We have used the method in a rather extensive study of the phase diagram for a molecular model of the water−methane system.[65] The method we present has two components. First, we make use of an isobaric semigrand ensemble in which the temperature, pressure, number of water molecules, and guest molecule chemical potential are fixed. Using Monte Carlo simulations in this ensemble, we determine the hydrate occupancy as a function of the guest molecule chemical potential. Thermodynamic integration is then used to determine the water chemical potential relative to that for the zero-occupancy hydrate as a function of the guest molecule chemical potential or hydrate occupancy. The second component of the method is a calculation of the zero-occupancy hydrate chemical potential. The zero-occupancy hydrate is not thermodynamically stable, but it is a reproducible, mechanically stable state in Monte Carlo simulations. Its Helmholtz free energy is determined using the method of Frenkel and Ladd,[66,67] involving an additional thermodynamic integration from a classical Einstein crystal reference state. This method is now the standard approach to determining the free energies of solids.[29,68−78] An alternative reference state for determining the water chemical potential as a function of the hydrate occupancy is the fully occupied hydrate. If the fully occupied hydrate is one where only single occupancy of the cavities is possible, then the system is a substitutionally ordered solid solution and its free energy may also be determined using the Frenkel−Ladd method.[69,71,79] A calculation of this latter type was presented by Baez[80] for a structure-I methane hydrate. However, in that calculation the large cages were fully occupied, leaving the small cages empty. This is a low-probability state, since all the cages of a structure-I methane hydrate are accessible to methane occupancy, and would not be suitable as a reference state.

As an illustration of the overall method, we apply it to two molecular models of the methane structure-I hydrate. The first is based on the primitive model of water/alkane mixtures developed by Nezbeda and co-workers.[81] This model features the primary physical effects governing hydrophobic hydration, i.e., one component forms a hydrogen bond network while the other does not, and it is of some interest to see whether the model generates stable hydrate phases. The second model is one where the water molecules interact via the simple point charge (SPC/E) model[82] and the methane molecules via the Lennard-Jones 12−6 potential. This can be regarded as a base case choice for a more realistic model of a hydrate. In addition to making it possible to calculate phase diagrams, the results from our methodology are also used to test the approximations in the vdWP theory and its extensions. Throughout this paper, we focus on the structure-I methane hydrate, but the methodology is applicable to any hydrate structure and to other guest molecules, and the extension to mixtures of guest molecules is straightforward.

In the next section of the paper, we discuss the methodology in more detail. In section III, we describe the molecular models used in our illustrative calculations. Section IV presents some results from the method calculations and includes thermodynamic consistency tests. In section V, we compare results from our calculations with predictions from the vdWP theory and its extensions, focusing on the predicted relationship between the occupancy and the methane chemical potential. Section 6 gives a summary of our results and conclusions.

II. Calculation of Free Energies and Chemical Potentials for Hydrate Phases

A. Semigrand Ensemble Calculation of Chemical Potentials for Hydrates. We begin with the fundamental property relationship for a binary mixture of water, w, and methane, m, expressed as

$$\mathrm{d}U = T\,\mathrm{d}S - P\,\mathrm{d}V + \mu_\mathrm{m}\,\mathrm{d}N_\mathrm{m} + \mu_\mathrm{w}\,\mathrm{d}N_\mathrm{w} \tag{1}$$

where μ is the chemical potential, N denotes numbers of molecules, S is the entropy, T is the temperature, and U is the internal energy. Taking the Legendre transform of U with respect to S, V, and N_m, we find

$$\mu_\mathrm{w}N_\mathrm{w} = U - TS + PV - \mu_\mathrm{m}N_\mathrm{m} \tag{2}$$

Taking the differential of eq 2, holding N_w constant, and using eq 1, we have

$$N_\mathrm{w}\,\mathrm{d}\mu_\mathrm{w} = -S\,\mathrm{d}T + V\,\mathrm{d}P - N_\mathrm{m}\,\mathrm{d}\mu_\mathrm{m} \tag{3}$$

We integrate eq 3 at fixed T and P to obtain the chemical potential of water relative to that in a reference state as

$$\mu_\mathrm{w} - \mu_\mathrm{w}^{(0)} = -\frac{1}{N_\mathrm{w}}\int_{\mu_\mathrm{m}^{(0)}}^{\mu_\mathrm{m}} N_\mathrm{m}\,\mathrm{d}\mu'_\mathrm{m} \tag{4}$$

The reference state in our calculations is typically the zero-occupancy hydrate so that $\mu_\mathrm{m}^{(0)} = -\infty$. The Gibbs free energy for the hydrate is given by

$$G = N_\mathrm{m}\mu_\mathrm{m} + N_\mathrm{w}\mu_\mathrm{w}^{(0)} - \int_{\mu_\mathrm{m}^{(0)}}^{\mu_\mathrm{m}} N_\mathrm{m}\,\mathrm{d}\mu'_m \tag{5}$$

N_m is obtained as an ensemble average by carrying out semigrand Monte Carlo (SGMC) simulations of the hydrate. The probability of configurations in the SGMC simulations is given by

$$p(V, N_\mathrm{m}, \boldsymbol{s}^N) \propto \frac{V^N}{N!}\exp\left(\frac{-PV}{kT}\right)\exp\left(\frac{N_\mathrm{m}\mu_\mathrm{m}}{kT}\right)\exp\left(\frac{-U(\boldsymbol{s}^N)}{kT}\right) \tag{6}$$

where $\boldsymbol{s}^N$ denotes the set of coordinates of the molecules, with translational coordinates scaled by $V^{1/3}$.

B. Free Energy of the Zero-Occupancy Hydrate. The zero-occupancy hydrate may be viewed as a metastable ice phase, and we use the Frenkel−Ladd (FL) method[66] to calculate its Helmoltz free energy. Our use of the FL method follows closely the original work, with modifications to treat the orientational degrees of freedom[83] and the effect of a fixed center of mass.[67] The starting point is defining the Einstein crystal Hamiltonian

$$H_E(\lambda_T, \lambda_R) = \sum_{i=1}^{N} \left[\lambda_T (\boldsymbol{R}_i - \boldsymbol{R}_i^{(0)})^2 + \lambda_R \left(\sin^2 \varphi_{a,i} + \left(\frac{\varphi_{b,i}}{\pi} \right)^2 \right) \right] \quad (7)$$

where λ_T and λ_R are force constants, $\boldsymbol{R}_i$ gives the Cartesian coordinates of molecule i, and $\boldsymbol{R}_i^{(0)}$ gives those coordinates for molecule i in a reference lattice. $\varphi_{a,i}$ and $\varphi_{b,i}$ are angles describing the orientational displacement of the molecules with respect to the reference lattice, and are described in more detail by Vega and Monson.[83] Equation 7 defines a classical Einstein crystal with a free energy that can be determined by a combination of analytical and numerical methods. If we add eq 7 to the Hamiltonian, H_0, for our model system of interest, we have the Hamiltonian for an interacting Einstein crystal

$$H_{IE}(\lambda_T, \lambda_R) = H_0 + H_E(\lambda_T, \lambda_R) \quad (8)$$

For very large values of λ_T and λ_R, the system behaves as an Einstein crystal that is only slightly perturbed by the interactions in H_0. For zero values of λ_T and λ_R, the system behavior is determined only by H_0. Thermodynamic integration is used to determine the free energy change associated with changing the force constants from zero to values sufficiently large, where the system is close to being an Einstein crystal.[66] We write the free energy of our system as

$$A = A_E + (A_{IE} - A_E) + (A_{CM} - A_{IE}) + (A - A_{CM}) \quad (9)$$

where A_E is the free energy of the Einstein crystal, A_{IE} is the free energy of an interacting Einstein crystal (i.e., the system with Hamiltonian $H_{IE}(\lambda_T, \lambda_R)$), and A_{CM} is the free energy of the hydrate but with its center of mass fixed. All quantities except A in eq 9 refer to systems with fixed center of mass. A_E can be written as $A_E = A_{E,T} + A_{E,R}$ where

$$A_{E,T} = -kT \ln \left[N^{-3/2} \left(\frac{\pi kT}{\lambda_T} \right)^{3(N-1)/2} \right] \quad (10)$$

is the contribution from translational motion,[67] and

$$A_{E,R} = -NkT \ln \left\{ \int_0^1 \exp \left[-\frac{\lambda_R}{kT} (1 - y^2) \right] dy \int_0^1 \exp \left[-\frac{\lambda_R}{kT} y'^2 \right] dy' \right\} \quad (11)$$

is the contribution from the rotational motion with $y = \cos \alpha$ and $y' = (\gamma/\pi)$ where α and γ refer to Euler angles describing the molecular orientation.[83] The difference in free energy between an noninteracting and interacting Einstein crystal is found by using

$$A_{IE} - A_E = -kT \ln \left\langle \exp \left[\frac{H_0}{kT} \right] \right\rangle_{H_E(\lambda_T, \lambda_R)} \quad (12)$$

with $\langle \rangle_{H_E(\lambda_T, \lambda_R)}$ indicating a canonical ensemble average evaluated for a system with Hamiltonian $H_E(\lambda_T, \lambda_R)$. The third term in eq 9 is determined using a coupling parameter integration over λ_T and λ_R.[66,68,83] The final term in eq 9 is given by $A - A_{CM} = \ln(V/N)$.[67] We assume that the hydrate is proton-disordered but that the contribution to the free energy from the disorder is independent of the molecular interactions and approximated by the residual entropy of ice as determined by Nagle.[84] The coordinates of the oxygen atoms for the perfect crystal used in specifying $H_E(\lambda_T, \lambda_R)$ are those given for the structure-I hydrate by McMullan and Jeffrey.[8] The orientations associated with the perfect crystal were determined by carrying out a search over the water molecule orientations to determine the configuration of lowest potential energy as discussed further in the next section.

III. Molecular Models and Monte Carlo Simulations

We have considered two types of models in this work. The first model was chosen in answer to the question of what might be the simplest molecular model that could describe hydrate behavior.[65] This is a mixture of a hard spheres representing the methane molecule and associating hard spheres (primitive model of water, PW) representing water—we refer to this as the PW/HS model. This model has been used extensively by Nezbeda and co-workers[81,85] in applications to aqueous solutions of alkanes, and the solid-fluid equilibrium of the PW has been previously studied for two ice phases.[86] The PW/HS model has hard sphere diameters, σ and σ_m, for water and methane, respectively, and we primarily use $\sigma_m = 1.25\sigma$. The PW model has four tetrahredrally coordinated square well sites, two sites labeled A and two labeled B, with range, $\lambda_w = 0.15\ \sigma$, and well depth, ϵ. The square well interactions occur only between an A site on one molecule and a B site on another, and only one bonding interaction can occur between each pair of sites. The second model we consider is similar to models that have been used in previous molecular simulation studies of hydrates.[37,48−63] We use a Lennard-Jones 12−6 potential for the methane−methane and methane−water interactions and the SPC/E[82] model for the water−water interactions. We refer to this as the SPCE/12−6 model. The methane−methane well depth and collision diameter parameters used here are $\epsilon_{mm}/k = 148$ K, $\sigma_{mm} = 0.373$ nm.[87] The methane−water parameters were $\epsilon_{mw}/k = 108$ K, $\sigma_{mw} = 0.344$ nm.

The Monte Carlo simulations of the SPCE/12−6 model included standard Ewald summation methods[88,89] to account for long-range electrostatic interactions. We used a convergence parameter of $5.5/L$, where L is the lattice parameter of a structure-I hydrate. The long-range dispersion interactions were also treated with a lattice summation method.[90] The initial water molecule configuration for the PW/HS model was obtained through simulated annealing by fixing the oxygen atom coordinates[8] and rotating the water molecules until a complete hydrogen-bonded network was found. A similar procedure was employed to obtain an initial configuration for the SPCE/12−6 model, with the objective being to minimize both the energy and the dipole moment of the hydrate unit cell. In this case, we used an annealing schedule with 20 temperatures in the range 400−0.1 K, with 10^6 cycles of rotation moves at each temperature, and we iterated each series of temperatures 10 times.

Our Monte Carlo simulations were carried out using the canonical, isobaric−isothermal, semigrand, and isobaric semigrand ensembles using the standard implementations of these ensembles. The simulations were typically run over 5×10^5 cycles with the first 10^5 cycles used for equilibration. In each case, a cycle consisted of $N = N_w + N_m$ attempted configuration changes. Five types of configuration changes were used: translations, rotations (water molecules only), insertions of methane molecules (semigrand simulations), deletions of methane molecules (semigrand simulations), and volume changes (isobaric simulations). The volume changes were attempted with probability $1/N$, while all other moves were attempted with equal probability. The system sizes consisted of either one or eight hydrate unit cells. Results presented here are for eight unit cells. The semigrand ensemble simulations were conducted over a range of μ_m starting with states in the neighborhood of the zero-

occupancy hydrate and finishing at a fully occupied hydrate. Integration of eq 4 is performed using the trapezoidal rule with equal intervals ($\delta\mu_m/kT$) = 0.05. In our FL method calculations, $A_{CM} - A_{IE}$ was determined using a ten-point Gaussian quadrature. For the interacting Einstein crystal, we used $\lambda_T/(kT\sigma^2)$ = 20 000 and λ_R/kT = 20 000, for the PW/HS model and $\lambda_T/(kT\text{Å}^2)$ = 20 000 and λ_R/kT = 20 000 for the SPCE/12−6 model.

IV. van der Waals−Platteeuw Theory

We give a review of the vdWP theory as context for the comparison of the results from this theory with our Monte Carlo simulations, highlighting the key approximations used. A useful starting point for considering this theory is the semigrand partition function for binary mixture of water and methane represented as

$$\Gamma(N_w, \mu_m, T, V) = \sum_{N_m=0}^{\infty} \lambda_m^{N_m} Q(N_w, N_m, V, T) \tag{13}$$

where

$$Q(N_w, N_m, V, T) = q_m^{N_m} q_w^{N_w} Z(N_w, N_m, V, T) \tag{14}$$

is the canonical partition function for the hydrate, q_i denotes the contribution to the molecular partition function for species i from internal degrees of freedom, and $\lambda_m = \exp(\mu_m/kT)$ is the activity of methane. $Z(N_w, N_m, V, T)$, the configurational partition function for the hydrate, is given by

$$Z(N_w, N_m, V, T) = \frac{1}{N_m! N_w!} \int \cdots \int e^{-\beta[U_{mm}+U_{mw}+U_{ww}]} d\mathbf{r}_1^{(m)} \ldots d\mathbf{r}_{N_m}^{(m)}, d\mathbf{r}_1^{(w)} \ldots d\mathbf{r}_{N_w}^{(w)} \tag{15}$$

where U_{ij}'s denote the contributions to the N-particle potential energy from the interaction between species i and j and we are assuming pairwise additivity. $\mathbf{r}_i^{(j)}$ denotes the set of coordinates of molecule i of type j, including orientations for the case of the water molecules. Equation 13 can be rewritten as

$$\Gamma(N_w, \mu_m, T, V) = Q(N_w, V, T) \sum_{N_m=0}^{\infty} z_m^{N_m} \frac{Z(N_w, N_m, V, T)}{Z(N_w, V, T)} \tag{16}$$

where

$$Q(N_w, V, T) = q_w^{N_w} Z(N_w, V, T) \tag{17}$$

and

$$Z(N_w, V, T) = \frac{1}{N_w!} \int \cdots \int e^{-\beta U_{ww}} d\mathbf{r}_1^{(w)} \ldots d\mathbf{r}_{N_w}^{(w)} \tag{18}$$

denote the canonical partition function and configurational partition function for the zero-occupancy hydrate structure, and $z_m = q_m\lambda_m$. The ratio $Z(N_w, N_m, V, T)/Z(N_w, V, T)$ can be expressed as

$$\frac{Z(N_w, N_m, V, T)}{Z(N_w, V, T)} = \frac{1}{N_m!} \left\langle \int \cdots \int e^{-\beta[U_{mm}+U_{mw}]} d\mathbf{r}_1^{(m)} \ldots d\mathbf{r}_{N_m}^{(m)} \right\rangle_w \tag{19}$$

where $\langle\rangle_w$ denotes an ensemble average over configurations of the water molecules. For a frozen configuration of the water molecules, this expression can be approximated by

$$\frac{Z(N_w, N_m, V, T)}{Z(N_w, V, T)} = Z^{(0)}(N_w, N_m, V, T) \frac{1}{N_m!} \int \cdots \int e^{-\beta[U_{mm}+U_{mw}^{(0)}]} d\mathbf{r}_1^{(m)} \ldots d\mathbf{r}_{N_m}^{(m)} \tag{20}$$

where $Z^{(0)}(N_w, N_m, V, T)$ is the configurational partition function for the methane molecules in the presence of an external field generated by the water molecules in a frozen configuration, and $U_{mw}^{(0)}$ denotes the methane−water interactions for this frozen water molecule configuration and is expressed as

$$U_{mw}^{(0)} = \sum_{i=1}^{N_m} \phi(\mathbf{r}_i) \tag{21}$$

where $\phi(\mathbf{r}_i)$ is the interaction energy of a single methane molecule with the water molecules. Equation 16 then becomes

$$\Gamma(N_w, \mu_m, T, V) = Q(N_w, V, T) \sum_{N_m=0}^{\infty} z_m^{N_m} Z^{(0)}(N_w, N_m, V, T) \tag{22}$$

The next step is to neglect the methane−methane interactions in the hydrate so that we can factorize eq 20 into a product of cell partition functions, each associated with a single methane molecule in a cell. For structure-I, we have two kinds of cells, associated with the large and small cavities, respectively. We can then write $Z^{(0)}(N_w, N_m, V, T)$ as a restricted sum of products of N_m cell partition functions as follows

$$Z^{(0)}(N_w, N_m, V, T) = \sum_{n_1^{(L)}=0}^{1*} \cdots \sum_{n_{M_L}^{(L)}=0}^{1*} \sum_{n_1^{(S)}=0}^{1*} \cdots \sum_{n_{M_S}^{(S)}=0}^{1*} [Z_1^{(L)}]^{(\sum_i^{M_L} n_i^{(L)})} [Z_1^{(S)}]^{(\sum_i^{M_S} n_i^{(S)})} \tag{23}$$

where $n_i^{(L)}$ denotes the number of methane molecules in large cage i, $n_i^{(S)}$ denotes the number of methane molecules in small cage i, and M_S and M_L are the numbers of small and large cages, respectively. The *'s on the summations denote the restriction that

$$\sum_i^{M_S} n_i^{(S)} + \sum_i^{M_L} n_i^{(L)} = N_m \tag{24}$$

The cell partition functions are given by

$$Z_1^{(j)} = \int e^{-\beta\phi^{(j)}(r_1)} d\mathbf{r}_1 \tag{25}$$

These are evaluated in our work via Monte Carlo integration. The right-hand side of eq 23 can be written as a restricted double binomial expansion

$$Z^{(0)}(N_w, N_m, V, T) = \sum_{n_L=0}^{M_L*} \sum_{n_S=0}^{M_S*} \frac{M_L!}{n_L!(M_L - n_L)!} (Z_1^{(L)})^{n_L} \frac{M_S!}{n_S!(M_S - n_S)!} (Z_1^{(S)})^{n_S} \tag{26}$$

where n_L denotes the number of methane molecules in large

cages i, n_S denotes the number of methane molecules in small cages, and the *'s on the summations now denote the restriction that $n_L + n_S = N_m$. Substituting eq 26 into eq 22 and summing over N_m gives

$$\Gamma(N_w, \mu_m, T, V) = Q_{N_w}(1 + z_m Z_1^{(L)})^{M_L} (1 + z_m Z_1^{(S)})^{M_S} \quad (27)$$

Notice that, once a static configuration of water molecules is assumed, and methane−methane interactions neglected, the factorization into cell partition functions is exact and not an additional approximation. We can obtain average number of methane molecules in the hydrate from

$$\langle N_m \rangle = z_m \left(\frac{\partial \ln \Gamma}{\partial z_m}\right)_{V,T} = \frac{M_L z_m Z_1^{(L)}}{1 + z_m Z_1^{(L)}} + \frac{M_S z_m Z_1^{(S)}}{1 + z_m Z_1^{(S)}} \quad (28)$$

and the fractional occupancy as

$$\Theta = \frac{\nu_L z_m Z_1^{(L)}}{1 + z_m Z_1^{(L)}} + \frac{\nu_S z_m Z_1^{(S)}}{1 + z_m Z_1^{(S)}} \quad (29)$$

where ν_L and ν_S are the fractions of large and small cages, respectively.

In the original version of the vdWP theory, $Z_1^{(S)}$ and $Z_1^{(L)}$ are approximated by treating the cages as spherical cavities and averaging interactions between the methane molecules in the cage and the closest shell of water molecules.[26,27] Subsequent workers have included longer-range methane−water interactions in the computation of $Z_1^{(S)}$ and $Z_1^{(L)}$.[30−37] The effect of the methane−methane interactions can be included through a mean field approximation[42,91] so that

$$\Theta = \frac{\nu_L z_m \exp(-\beta\Theta a_L) Z_1^{(L)}}{1 + z_m \exp(-\beta\Theta a_L) Z_1^{(L)}} + \frac{\nu_S z_m \exp(-\beta\Theta a_S) Z_1^{(S)}}{1 + z_m \exp(-\beta\Theta a_S) Z_1^{(S)}} \quad (30)$$

where a_L and a_S are the interaction energies between methane molecules at the centers of large and small cages, respectively, and those at the centers of nearest-neighbor cages. Equation 30 can be solved for Θ by iteration. By computing the hydrate occupancies exactly for given intermolecular potential models using Monte Carlo simulations, we can assess the accuracy of assumptions in the vdWP theories. In our calculations with vdWP theories the long-range dispersion interactions were treated with a static lattice summation over $5 \times 5 \times 5$ unit cells, which was sufficient to converge the summations.

V. Results and Discussion

A. Free Energies and Chemical Potentials. We first consider the calculations of the free energies and chemical potentials for the PW/HS model. We have calculated the free energy for the hydrate in the fully occupied and zero-occupancy states and have also calculated the free energy difference between these states using thermodynamic integration of SGMC simulation results for the occupancy versus methane chemical potential. Typical results from these latter calculations are shown in Figure 1 which shows the occupancy of the hydrate versus the methane chemical potential. Figure 2 shows the methane and water chemical potentials versus the methane mole fraction calculated from the results in Figure 1. We note that the methane chemical potential becomes increasingly positive as the hydrate is filled with methane, or equivalently as seen in Figure 1, the occupancy reaches a plateau value as the chemical potential is progressively increased. The water chemical potential is less sensitive to the methane mole fraction, since the water density varies only slightly as the methane mole fraction increases. Table 1 shows results of a thermodynamic consistency test where we compare the free energy of the fully occupied hydrate calculated via thermodynamic integration from the zero-occupancy state with that calculated directly from the FL method. The agreement is excellent, indicating that these independent estimates of the free energy are thermodynamically consistent.

Figure 3 shows results for the Gibbs energy versus the composition for the PW/HS model of the hydrate for various

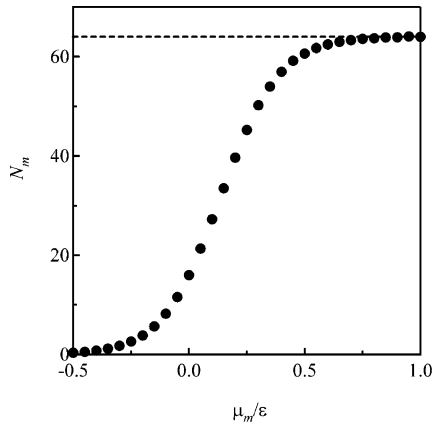

Figure 1. Semigrand ensemble average of the number of methane molecules, N_m, vs chemical potential, μ_m/ϵ for an eight unit cell of the PW/HS hydrate. The maximum occupancy of N_m is 64 as shown by the leveling-off of N_m with increasing μ_m.

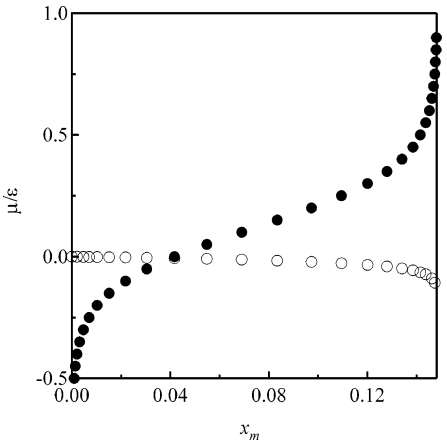

Figure 2. Chemical potentials of water, $\mu_w - \mu_w^{(0)}$ (open symbols), and methane, μ_m (filled symbols), in the PW/HS hydrate vs composition of methane molecules, x_m.

TABLE 1: A Test of the Thermodynamic Consistency of the Method for the PW/HS Model with $\sigma_m = 1.25\sigma$[a]

		$G/N\epsilon$		
kT/ϵ	$P\sigma^3/\epsilon$	zero-occupancy hydrate (FL)	full hydrate (FL)	full hydrate (TI)
0.10	0.0083	−0.548(3)	−0.453(3)	−0.449(3)
0.10	0.8333	0.972(4)	0.846(4)	0.848(3)
0.12	0.0100	−0.255(4)	−0.200(4)	−0.197(4)
0.12	1.0000	1.568(4)	1.356(5)	1.360(4)

[a] Results for the Gibbs free energy are shown for the zero-occupancy hydrate and the fully occupied hydrate calculated from the FL method. The Gibbs free energy of the full hydrate calculated using thermodynamic integration (TI) from the zero-occupancy hydrate reference state via eq 5 is also shown. All simulations were performed on an eight unit cell hydrate.

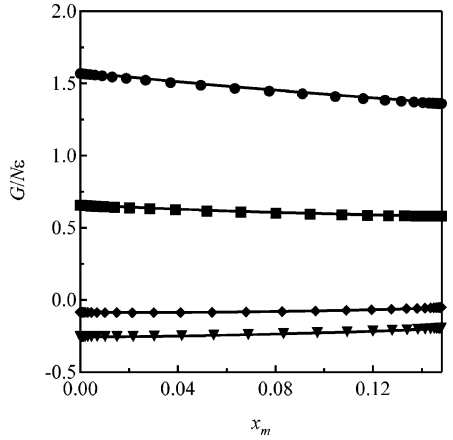

Figure 3. Gibbs free energy, $G/N\epsilon$ as a function of composition at $kT/\epsilon = 0.12$ for the PW/HS hydrate. From bottom to top, $P\sigma^3/\epsilon$ has been fixed at 0.01, 0.10, 0.50, and 1.0. The markers indicate simulation results from the combination of the FL method and constant pressure SGMC simulation results. The lines are fits of the data (see ref 61).

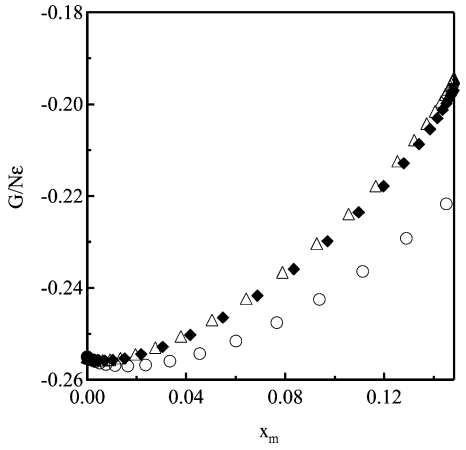

Figure 4. Dependence of the Gibbs free energy on solute radius at $kT/\epsilon = 0.12$ and $P\sigma^3/\epsilon = 0.01$ for the PW/HS hydrate. The radii are set to 1.0 σ_w (circles), 1.25 σ_w (diamonds), and 1.27 σ_w (triangles).

pressures. The lines in these plots are fits to the simulation results that are described elsewhere[65] where we use them in calculations of hydrate phase diagrams. We see that the Gibbs energy increases with pressure at fixed composition as would be expected—the spacing of these curves indicates that the pressure dependence is approximately linear, reflecting the relative incompressibility of the hydrate. The composition dependence changes gradually as the pressure is changed, suggesting that the occupied hydrate becomes more stable with respect to the zero-occupancy hydrate as the pressure is increased.

It is also interesting to study the dependence of the hydrate free energy upon the size of the guest molecule. This is shown in Figure 4 which shows the free energy versus hydrate composition for three guest molecule sizes. The large change in $G/N\epsilon$ between $\sigma_m = 1.00$ and $\sigma_m = 1.25$ is mainly due to the loss of free volume for the larger guest molecule. At first glance, the gas hydrate with a smaller guest molecule might be expected to be more stable, but the contrary is found when solid−fluid equilibrium calculations are made[65] because of the impact of the molecular size on the fluid-phase free energy.

In Table 2, we present calculated properties for the SPCE/12−6 model for a hydrate at $T = 241.5$ K and $P = 102.9$ bar. Results are shown for the full and zero-occupancy hydrate states. The Gibbs energies for both states are shown calculated directly using the FL method, as well as for the full hydrate state

TABLE 2: Thermodynamic Properties for the SPCE/12−6 Methane Model at $T = 241.5$ K and $P = 102.9$ bar[a]

		G(kJ/mol)		
T(K)	P(bar)	zero-occupancy hydrate (FL)	full hydrate (FL)	full hydrate (TI)
241.5	102.9	−38.66(6)	−35.70(5)	−35.67(5)

[a] The final column gives the Gibbs free energy of the full hydrate calculated via thermodynamic integration starting from the zero-occupancy hydrate.

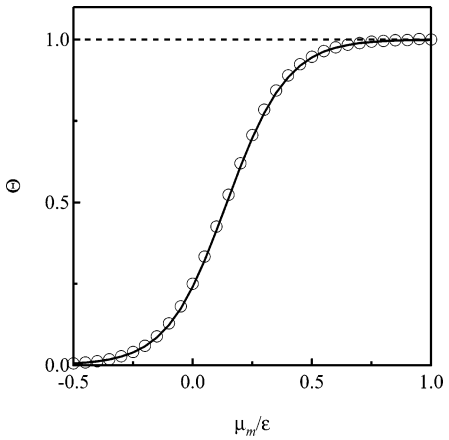

Figure 5. Fractional occupancy for the methane structure-I hydrate vs the methane chemical potential from the PW/HS model at $kT/\epsilon = 0.12$ and $P\sigma^3/\epsilon = 0.01$. Results from constant pressure SGMC calculations (open circles) are compared with the vdWP theory (line).

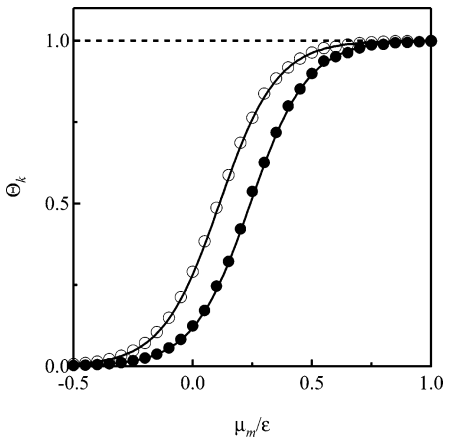

Figure 6. Fractional occupancies of the large and small cages in the methane structure-I hydrate vs the methane chemical potential from the PW/HS model at $kT/\epsilon = 0.12$ and $P\sigma^3/\epsilon = 0.01$. Results from constant pressure SGMC calculations for the small cages (filled circles) and the large cages (open circles) are compared with the vdWP theory (lines).

calculated via thermodynamic integration using the semigrand ensemble simulation results starting from a zero-occupancy hydrate reference state. The thermodynamic consistency of the results is again evident.

B. Comparisons with vdWP-Type Theories. We have made tests of the vdWP theory for both the PW/HS and SPCE/12−6 models. Figure 5 shows the fractional occupancy versus methane chemical potential for the PW/HS model, and Figure 6 shows the contributions from the large and small cages. Here, we see that the vdWP theory gives excellent agreement with the simulation results. This is in part due to the fact that the PW/HS model has no methane−methane interactions in the hydrate phase. When using this model in calculations of hydrate properties, we add the methane−methane interactions via a van

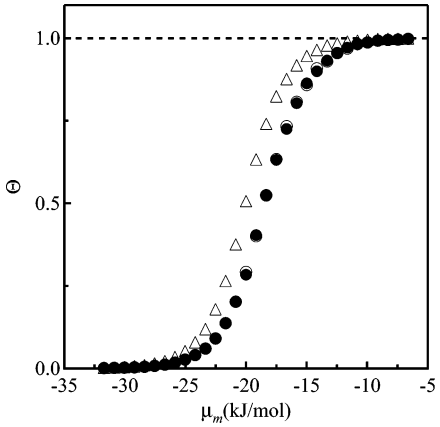

Figure 7. Fractional occupancy for the methane structure-I hydrate vs the methane chemical potential from the SPCE/12−6 model at $T = 241.5$ K and $P = 102.9$ bar. Results are shown from (i) constant pressure SGMC simulations (filled circles); (ii) constant volume SGMC simulations (open circles); (iii) SGMC simulations using a frozen configuration of water molecules (triangles).

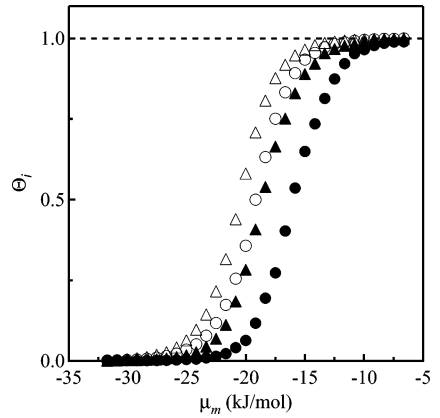

Figure 8. Fractional occupancies of the large and small cages for the methane structure-I hydrate vs the methane chemical potential from the SPCE/12−6 model at $T = 241.5$ K and $P = 102.9$ bar. Results are shown from (i) constant pressure SGMC simulations (filled circles, small cages; open circles, large cages); (ii) SGMC simulations using a frozen configuration of water molecules (open triangles, large cages; filled triangles, small cages).

der Waals mean field approximation.[65] In addition, the very strongly directional nature of the association interactions in the PW/HS model makes the hydrate framework a more rigid structure, so that the assumption of a frozen water molecule configuration is more accurate.

We now consider results for the SPCE/12−6 model. In this case, to test the theory we have carried out Monte Carlo simulations in three ways: (i) for a hydrate at fixed pressure; (ii) for a hydrate at a fixed volume given by the average volume from the fixed pressure simulation; (iii) for a hydrate with a fixed volume and frozen water molecule configuration. Figure 7 shows the hydrate fractional occupancy versus the methane chemical potential for these three cases. We see that there is only a slight difference between the results for the constant pressure and constant volume cases, but the occupancy is significantly higher when a frozen configuration of water molecules is used (a similar observation has very recently been made by Sisov and Piotrovskaya[64]). Figure 8 shows the corresponding results for the small- and large-cage fractional occupancies. Interestingly, we see that the effect of using a frozen water molecule configuration is greater for the smaller cages, reflecting the fact that the cage geometry is more sensitive to the water molecule configuration for the small cages.

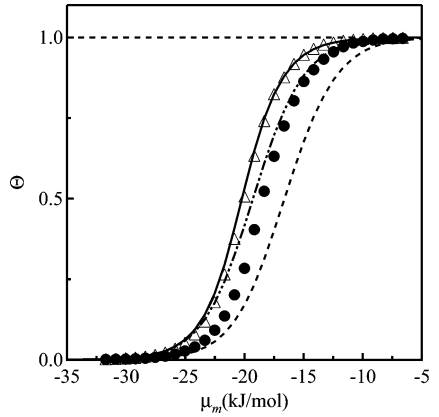

Figure 9. Fractional occupancy for the methane structure-I hydrate vs the methane chemical potential from the SPCE/12−6 model at $T = 241.5$ K and $P = 102.9$ bar. Results are shown from (i) constant pressure SGMC simulations (filled circles); (ii) SGMC simulations using a frozen configuration of water molecules (triangles); (iii) the original version of the vdWP theory, neglecting methane−methane interactions and methane−water interactions beyond the cage (dashed line); (iv) vdWP theory neglecting methane−methane interactions but including long-range methane−water interactions (dot-dashed line); (v) vdWP theory including methane−methane interactions via eq 30 and long-range methane−water interactions (full line).

Figure 9 shows a comparison of the simulation results for the SPCE/12−6 model hydrate with predictions from three versions of the vdWP theory: (i) the original version of the theory, neglecting methane−methane interactions and methane−water interactions beyond the cage; (ii) neglecting methane−methane interactions but including long-range methane−water interactions; (iii) including methane−methane interactions via eq 30 and long-range methane−water interactions. The closest agreement between theory and simulation is between the simulation results with a frozen water molecule configuration and the predictions of eq 30, where the long-range methane−methane and methane−water interactions are included. The closest agreement between theory and the most physically realistic simulation results (i.e., constant pressure simulations without restrictions on the water molecule coordinates) is for the version of the theory neglecting methane−methane interactions but including long-range methane−water interactions. Thus, there seems to be some cancellation of the error arising from the assumption of a fixed configuration of water molecules in the hydrate framework with that arising from the neglect of methane−methane interactions.

VI. Summary and Conclusions

We have presented a methodology for calculating the free energies and chemical potentials of gas hydrate systems from Monte Carlo simulations. The method combines the determination of the free energy of the zero-occupancy hydrate via the FL method with SGMC simulations to calculate free energy and chemical potential differences as a function of hydrate occupancy. We have presented sample calculations for this methodology for two models of the structure-I methane hydrate: (i) the PW/HS model, perhaps the simplest model that can describe hydrate stability;[65] (ii) the SPCE/12−6 model, which is potentially a more quantitatively realistic model.

Our sample calculations for the PW/HS model demonstrate that the method can be applied in a thermodynamically consistent way. For the structure-I methane hydrate, the FL method can be applied to both the zero-occupancy and fully occupied hydrate. Either one of these states can be used as a

reference state for calculating the free energies and chemical potentials as a function of hydrate occupancy from the SGMC simulations. For hydrate systems with significant multiple cage occupancy, the FL method cannot be used to obtain free energies for the fully occupied hydrate, since the guest molecules will not be translationally ordered. However, our methodology still works for such cases, because we can still use the zero-occupancy reference state for the thermodynamic integrations.

Our SGMC simulation results for the hydrate occupancy versus methane chemical potential for the structure-I methane hydrate provide useful information about the accuracy of the vdWP theory and its extensions. The original theory is accurate for the PW/HS model because of some intrinsic features of the model, especially the rigidity of the hydrate framework produced by that model. For the more realistic SPCE/12−6 model, the original vdWP theory is less accurate. Its predictions are improved by addition of long-range methane−water and methane−methane interactions. However, our results indicate that for this more realistic model the effects of allowing the water molecules to move are very important, and this is not included in the theories discussed here. The techniques used by Tanaka and co-workers,[41,43−46] based on lattice dynamics, may lead to more accurate results. One important observation in our work is the apparent cancellation of errors between the effects of water molecule motions and long-range methane−methane interactions.

The techniques used here have already been used in studies of the methane−water phase diagram using models based on the PW/HS model, including fluid, pure solid, and hydrate phases.[65] This work has shown that this simple model can reproduce all the qualitative features of the phase diagram. Phase diagram calculations for more realistic models with the goal of achieving more quantitative agreement with experimental phase behavior are underway.

Acknowledgment. The authors are grateful to Professor C. Vega for helpful discussions on the calculation of solid phase free energies for SPCE/12−6 model. This work was supported by a grant from the U.S. Department of Energy (contract no. DE-FG02-90ER14150).

References and Notes

(1) Sloan, E. D.; Koh, C. A. *Clathrate Hydrates of Natural Gases*, 3rd ed.; CRC Press: New York, 2007.
(2) Sloan, E. D. *Nature (London)* **2003**, *426* (6964), 353−359.
(3) Koh, C. A. *Chem. Soc. Rev.* **2002**, *31* (3), 157−167.
(4) Englezos, P. *Ind. Eng. Chem. Res.* **1993**, *32* (7), 1251−1274.
(5) Frost, E.; Deaton, W. M. *Oil Gas J.* **1946**, *45*, 175.
(6) Kobayashi, R.; Katz, D. L. *Ind. Eng. Chem.* **1953**, *45* (2), 440−446.
(7) Sloan, E. D.; Khoury, F. M.; Kobayashi, R. *Ind. Eng. Chem. Fund.* **1976**, *15* (4), 318−323.
(8) Mcmullan, R. K.; Jeffrey, G. A. *J. Chem. Phys.* **1965**, *42* (8), 2725.
(9) Makino, T.; Nakamura, T.; Sugahara, T.; Ohgaki, K. *Fluid Phase Equilib.* **2004**, *218* (2), 235−238.
(10) Cady, G. H. *J. Phys. Chem.* **1983**, *87* (22), 4437−4441.
(11) Handa, Y. P. *J. Phys. Chem.* **1986**, *90* (22), 5497−5498.
(12) Ceccotti, P. J. *Ind. Eng. Chem. Fund.* **1966**, *5* (1), 106.
(13) Sum, A. K.; Burruss, R. C.; Sloan, E. D. *J. Phys. Chem. B* **1997**, *101* (38), 7371−7377.
(14) Galloway, T. J.; Ruska, W.; Chappele, P.; Kobayashi, R. *Ind. Eng. Chem. Fund.* **1970**, *9* (2), 237.
(15) Uchida, T.; Okabe, R.; Gohara, K.; Mae, S.; Seo, Y.; Lee, H.; Takeya, S.; Nagao, J.; Ebinuma, T.; Narita, H. *Can. J. Phys.* **2003**, *81* (1−2), 359−366.
(16) Hirai, H.; Uchihara, Y.; Fujihisa, H.; Sakashita, M.; Katoh, E.; Aoki, K.; Yamamoto, Y.; Nagashima, K.; Yagi, T. *J. Phys.: Condens. Matter* **2002**, *14* (44), 11443−11446.
(17) Loveday, J. S.; Nelmes, R. J.; Klug, D. D.; Tse, J. S.; Desgreniers, S. *Can. J. Phys.* **2003**, *81* (1−2), 539−544.
(18) Sloan, E. D. *J. Chem. Thermodyn.* **2003**, *35* (1), 41−53.
(19) Huo, Z. X.; Hester, K.; Sloan, E. D.; Miller, K. T. *AIChE J.* **2003**, *49* (5), 1300−1306.
(20) Predota, M.; Nezbeda, I.; Cummings, P. T. *Mol. Phys.* **2002**, *100* (14), 2189−2200.
(21) Predota, M.; Nezbeda, I. *Mol. Phys.* **1999**, *96* (8), 1237−1248.
(22) Guillot, B.; Guissani, Y. *J. Chem. Phys.* **1993**, *99* (10), 8075−8094.
(23) Paschek, D. *J. Chem. Phys.* **2004**, *120* (14), 6674−6690.
(24) Koh, C. A.; Wisbey, R. P.; Wu, X. P.; Westacott, R. E.; Soper, A. K. *J. Chem. Phys.* **2000**, *113* (15), 6390−6397.
(25) Radhakrishnan, R.; Trout, B. L. *J. Chem. Phys.* **2002**, *117* (4), 1786−1796.
(26) van der Waals, J. H. *Trans. Faraday Soc.* **1956**, *52* (2), 184−193.
(27) Platteeuw, J. C.; Vanderwaals, J. H. *Recl. Trav. Chim. Pays-Bas* **1959**, *78* (2), 126−133.
(28) Barker, J. A. *Lattice theories of the liquid state;* Pergamon Press: Oxford, 1963.
(29) Monson, P. A.; Kofke, D. A. *Adv. Chem. Phys.* **2000**, *115*, 113−179.
(30) Tester, J. W.; Bivins, R. L.; Herrick, C. C. *AIChE J.* **1972**, *18* (6), 1220.
(31) Sparks, K. A.; Tester, J. W. *J. Phys. Chem.* **1992**, *96* (26), 11022−11029.
(32) Sparks, K. A.; Tester, J. W.; Cao, Z. T.; Trout, B. L. *J. Phys. Chem. B* **1999**, *103* (30), 6300−6308.
(33) Natarajan, V.; Bishnoi, P. R. *Ind. Eng. Chem. Res.* **1995**, *34* (4), 1494−1498.
(34) John, V. T.; Holder, G. D. *J. Phys. Chem.* **1981**, *85* (13), 1811−1814.
(35) John, V. T.; Holder, G. D. *J. Phys. Chem.* **1982**, *86* (4), 455−459.
(36) John, V. T.; Holder, G. D. *J. Phys. Chem.* **1985**, *89* (15), 3279−3285.
(37) Rodger, P. M. *J. Phys. Chem.* **1989**, *93* (18), 6850−6855.
(38) Anderson, B. J.; Bazant, M. Z.; Tester, J. W.; Trout, B. L. *J. Phys. Chem. B* **2005**, *109* (16), 8153−8163.
(39) Anderson, B. J.; Tester, J. W.; Trout, B. L. *J. Phys. Chem. B* **2004**, *108* (48), 18705−18715.
(40) Klauda, J. B.; Sandler, S. I. *J. Phys. Chem. B* **2002**, *106* (22), 5722−5732.
(41) Tanaka, H.; Nakatsuka, T.; Koga, K. *J. Chem. Phys.* **2004**, *121* (11), 5488−5493.
(42) Klauda, J. B.; Sandler, S. I. *Chem. Eng. Sci.* **2003**, *58* (1), 27−41.
(43) Tanaka, H.; Kiyohara, K. *J. Chem. Phys.* **1993**, *98* (5), 4098−4109.
(44) Tanaka, H.; Kiyohara, K. *J. Chem. Phys.* **1993**, *98* (10), 8110−8118.
(45) Tanaka, H. *J. Chem. Phys.* **1994**, *101* (12), 10833−10842.
(46) Tanaka, H.; Nakanishi, K. *Mol. Sim.* **1994**, *12* (3−6), 317−327.
(47) Westacott, R. E.; Rodger, P. M. *Chem. Phys. Lett.* **1996**, *262* (1−2), 47−51.
(48) Tse, J. S.; Klein, M. L.; McDonald, I. R. *J. Phys. Chem.* **1983**, *87* (21), 4198−4203.
(49) Tse, J. S.; Klein, M. L.; Mcdonald, I. R. *J. Chem. Phys.* **1983**, *78* (4), 2096−2097.
(50) Tse, J. S.; Klein, M. L.; McDonald, I. R. *J. Chem. Phys.* **1984**, *81* (12), 6146−6153.
(51) Tse, J. S. *J. Inclusion Phenom.* **1994**, *17* (3), 259−266.
(52) English, N. J.; MacElroy, J. M. D. *J. Comput. Chem.* **2003**, *24* (13), 1569−1581.
(53) Zele, S. R.; Lee, S. Y.; Holder, G. D. *J. Phys. Chem. B* **1999**, *103* (46), 10250−10257.
(54) Marchi, M.; Mountain, R. D. *J. Chem. Phys.* **1987**, *86* (11), 6454−6455.
(55) Moon, C.; Taylor, P. C.; Rodger, P. M. *J. Am. Chem. Soc.* **2003**, *125* (16), 4706−4707.
(56) Moon, C.; Taylor, P. C.; Rodger, P. M. *Can. J. Phys.* **2003**, *81* (1−2), 451−457.
(57) Chialvo, A. A.; Houssa, M.; Cummings, P. T. *J. Phys. Chem. B* **2002**, *106* (2), 442−451.
(58) Rodger, P. M. *Ann. N. Y. Acad. Sci.* **2000**, *912*, 474−482.
(59) Rodger, P. M. *J. Phys. Chem.* **1990**, *94* (15), 6080−6089.
(60) Rodger, P. M. *AIChE J.* **1991**, *37* (10), 1511−1516.
(61) Rodger, P. M.; Forester, T. R.; Smith, W. *Fluid Phase Equilib.* **1996**, *116* (1−2), 326−332.
(62) Yezdimer, E. M.; Cummings, P. T.; Chialvo, A. A. *J. Phys. Chem. A* **2002**, *106* (34), 7982−7987.
(63) Okano, Y.; Yasuoka, K. *J. Chem. Phys.* **2006**, *124* (2), 024510.
(64) Sisov, V. V.; Piotrovskaya, E. M. *J. Phys. Chem. B* **2007**, *111*, 2886−2890.
(65) Wierzchowski, S. J.; Monson, P. A. *Ind. Eng. Chem. Res.* **2006**, *45* (1), 424−431.
(66) Frenkel, D.; Ladd, A. J. C. *J. Chem. Phys.* **1984**, *81* (7), 3188−3193.

(67) Polson, J. M.; Trizac, E.; Pronk, S.; Frenkel, D. *J. Chem. Phys.* **2000**, *112* (12), 5339−5342.
(68) Vega, C.; Paras, E. P. A.; Monson, P. A. *J. Chem. Phys.* **1992**, *96* (12), 9060−9072.
(69) Schroer, J. W.; Monson, P. A. *J. Chem. Phys.* **2003**, *118* (6), 2815−2823.
(70) Malanoski, A. P.; Monson, P. A. *J. Chem. Phys.* **1999**, *110* (1), 664−675.
(71) Cao, M.; Monson, P. A. *J. Chem. Phys.* **2005**, *122* (5), 054505.
(72) Sanz, E.; Vega, C.; Abascal, J. L. F.; MacDowell, L. G. *Phys. Rev. Lett.* **2004**, *92* (25), 255701.
(73) Meijer, E. J.; Frenkel, D.; Lesar, R. A.; Ladd, A. J. C. *J. Chem. Phys.* **1990**, *92* (12), 7570−7575.
(74) Polson, J. M.; Frenkel, D. *J. Chem. Phys.* **1998**, *109* (1), 318−328.
(75) Polson, J. M.; Frenkel, D. *J. Chem. Phys.* **1999**, *111* (4), 1501−1510.
(76) Arbuckle, B. W.; Clancy, P. *J. Chem. Phys.* **2002**, *116* (12), 5090−5098.
(77) Gao, G. T.; Zeng, X. C.; Tanaka, H. *J. Chem. Phys.* **2000**, *112* (19), 8534−8538.
(78) Baez, L. A.; Clancy, P. *Mol. Phys.* **1995**, *86* (3), 385−396.
(79) Eldridge, M. D.; Madden, P. A.; Frenkel, D. *Nature (London)* **1993**, *365* (6441), 35−37.
(80) Baez, L. A. *Computer simulation of early-stage crystal growth and dissolution*. Ph.D. thesis, Cornell University, 1996.
(81) Nezbeda, I.; Smith, W. R.; Kolafa, J. *J. Chem. Phys.* **1994**, *100* (3), 2191−2201.
(82) Berendsen, H. J. C.; Grigera, J. R.; Straatsma, T. P. *J. Phys. Chem.* **1987**, *91* (24), 6269−6271.
(83) Vega, C.; Monson, P. A. *J. Chem. Phys.* **1999**, *109* (22), 9938−9949.
(84) Nagle, J. F. *J. Math. Phys.* **1966**, *7* (8), 1484.
(85) Nezbeda, I.; Kolafa, J.; Pavlicek, J.; Smith, W. R. *J. Chem. Phys.* **1995**, *102* (24), 9638−9646.
(86) Vega, C.; Monson, P. A. *J. Chem. Phys.* **1998**, *109* (22), 9938−9949.
(87) Jorgensen, W. L. *J. Am. Chem. Soc.* **1981**, *103*, 335.
(88) Heyes, D. M. *Phys. Rev. B* **1994**, *49* (2), 755−764.
(89) Nymand, T. M.; Linse, P. *J. Chem. Phys.* **2000**, *112* (14), 6152−6160.
(90) Lopez-Lemus, J.; Alejandre, J. *Mol. Phys.* **2003**, *101* (6), 743−751.
(91) Klauda, J. B.; Sandler, S. I. *Mar. Pet. Geol.* **2003**, *20* (5), 459−470.